TEST RESULTS OF CHORDWISE AND SPANWISE BLOWING FOR LOW-SPEED LIFT AUGMENTATION

G. A. Howell*
General Dynamics, Fort Worth Division
Fort Worth, Texas

ABSTRACT

Low-speed wind tunnel tests were conducted on a large-scale and a small-scale powered model of a STOL wing/canard concept with engines mounted over the wing. In a basic configuration, both models exhausted the entire nozzle-flow momentum over vectoring flaps. In an alternate configuration, both models exhausted a portion of the flow from spanwise nozzles in the outer nacelle wall to obtain wing-leading-edge vortex augmentation. Force and pressure data were obtained for the small-scale model powered by compressed air. Pressure and thermal data were obtained for the large-scale model powered by two turbojet engines. Chordwise blowing decreased the pressures over the entire wing upper surface and even on the canard at high angles of attack. The power-induced lift coefficients were moderate for chordwise blowing. Spanwise blowing increased the strength of the wing leading-edge vortex and reduced the pressure on the wing upper surface beneath the path of the vortex.

NOMENCLATURE

A_e	Nozzle exit area
A_t	Nozzle throat area
C_D	Drag coefficient
C_ℓ	Section lift coefficient
C_L	Lift coefficient
C_M	Pitching moment coefficient
C_P	Pressure coefficient
C_T	Thrust coefficient
H	Total pressure (psf)
T	Thrust (lb)
(x/c)cp	Section center of pressure
CWB	Chordwise blowing
NPR	Nozzle pressure ratio
SWB	Spanwise blowing
α	Angle of attack
δ_{TE}	Wing trailing-edge flap deflection (deg)
ΔC_L	Power-induced lift coefficient
ΔT	Temperature rise (^oF)
Θ_j	Jet deflection angle (deg)

* Engineering Specialist

INTRODUCTION

Future battle scenarios place stringent requirements on tactical fighter aircraft if they are to survive and operate effectively against the severe threats they will likely encounter. One of the foremost threats, runway denial, can be effectively countered by STOL capability. The desire to add this capability to next-generation fighters has stimulated an increase in research efforts to provide the technologies for improving aircraft performance in this critical area. General Dynamics research has led to the development of a unique concept in which the propulsion system is integrated with the airframe to provide thrust vectoring as well as an improvement in the aerodynamic characteristics through power-induced effects. This concept, designated Vectored-Engine-Over-Wing (VEO-Wing), offers the potential for superior STOL capability while retaining good transonic and supersonic characteristics.

Earlier studies experimentally investigated the subsonic, transonic, and supersonic aerodynamic characteristics of the VEO-Wing concept.[1, 2, 3, 4] The experimental data base was later used in a study of this concept applied to a supersonic fighter in an air-to-ground role.[5] It was shown that a VEO-Wing design would have a significantly lower gross weight than a conventional design for STOL capability of less than 1000 ft.

The VEO-Wing concept was recently evaluated in low-speed tests of a small-scale and a large-scale model. The small-scale model was tested in a cooperative program conducted by the NASA Langley Research Center, the U.S. Air Force Flight Dynamics Laboratory, and General Dynamics.[6] The large-scale model was designed, fabricated, and tested by the NASA Ames Research Center.[7, 8] Key findings from these tests are presented in this paper with emphasis on the power effects on the wing and canard flowfields and on the power-induced lift.

DESCRIPTION OF MODELS AND TESTS

Large-Scale Model

The NASA Ames Research Center's STOL fighter model was used in the acquisition of most of the pressure data presented in this paper. A photograph of this model is shown in Figure 1; several of the geometric characteristics are listed in Table 1. This large-scale model, sized to accommodate two J-97 turbojet engines mounted in the podded nacelles, is approximately a 75% scale of an operational fighter aircraft designed to perform an air-superiority mission. The effects of power are discussed in this paper with variations of the trailing-edge flap only, although the model was equipped with a full set of variable control surfaces to simulate maneuver and STOL conditions.

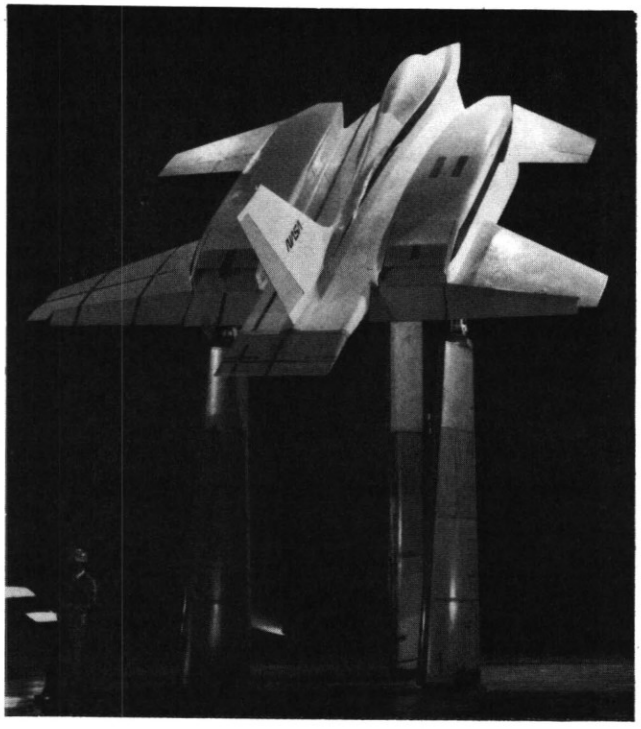

Figure 1 NASA Ames Research Center's Large-Scale STOL Fighter Model

TABLE 1

GEOMETRIC CHARACTERISTICS OF THE LARGE-SCALE MODEL

FUSELAGE	
Length	33.6 ft
WING	
Planform Area	182.0 ft^2
Span	23.9 ft
Leading-edge Sweep	40 deg
Aspect Ratio	3.13
Taper Ratio	.24
Twist	-4^o
Airfoil Section	NACA 64A204
CANARD	
Planform Area	38.0 ft^2
Span	19.8 ft.
Leading-edge Sweep	45 deg
Aspect Ratio	2.07
Taper Ratio	.42
Airfoil Section	NACA 64A004

The model's two-dimensional, half-wedge, convergent-divergent nozzle turned the flow downward at an angle of 25 deg before it passed through the exit plane. The nozzle exit was positioned at the hingeline of the wing inboard trailing-edge flap, and the engine exhaust flowed over this segment of the flap, which served as a thrust vectoring device by turning the exhaust flow. The spanwise blowing feature employed nozzles located in the sidewall of the nacelle to direct a portion of the total exhaust airflow over the wing. These were rectangular nozzles with an aspect ratio of 4.0 and an exit area of 20 in^2. The exit area of each chordwise nozzle was reduced from 120 in^2 to 100 in^2 when the spanwise nozzles were installed to maintain a constant total exit area. The spanwise nozzles, which accounted for 17% of the total exit area, were mounted approximately 1.5 nozzle heights above the wing surface with the nozzle forward edge located at the 23% exposed wing root chord. The complete propulsion system and the thrust and flow turning characteristics are discussed in a NASA report[9]; preliminary force data are presented in an AIAA paper.[10]

Pressure instrumentation (Figure 2) included two chordwise rows of pressure orifices on the wing upper and lower surfaces, one spanwise row at the mid-chord of the wing upper surface, and single chordwise rows on the upper and lower surfaces of the canard. Thermocouples were installed on the wing upper surface along the chordwise and spanwise pressure rows to measure the heating effects of the spanwise jet.

Aerodynamic data on the STOL fighter model were obtained in the 40- by 80-Foot Wind Tunnel at the NASA Ames Research Center. The angle of attack was varied from -8 deg to 36 deg, and the tunnel dynamic pressure for the data presented here was near 20 psf. The power-on runs were conducted at a nominal NPR of 2.0, which produced a thrust of approximately 2000 lb per engine and an exhaust temperature near 1100°F.

Small-Scale Model

The General Dynamics' VEO-Wing research model was tested to determine the effects of power on the aerodynamic forces. This model, shown in Figure 3, is approximately a 10.8% scale of an air-superiority fighter. Some of the geometric characteristics are listed in Table 2. Since it was developed as a low-cost research tool, the fuselage was simulated by a circular cylinder and the vertical tail was omitted. Power was supplied to the model by high-pressure air that passed through the sting into a plenum chamber in the circular fuselage. The air supply was then routed through tubes in the strake, through a choke plate in the nacelle, and into a small plenum chamber just upstream of the nozzle. This arrangement required that the inlet be faired over. Complete details of this model are provided in a General Dynamics report.[11] The small-scale model was also equipped with a full set of variable control surfaces, but to maintain consistency with the data presentation for the large-scale model, the effects of power are discussed only at two wing trailing-edge flap settings.

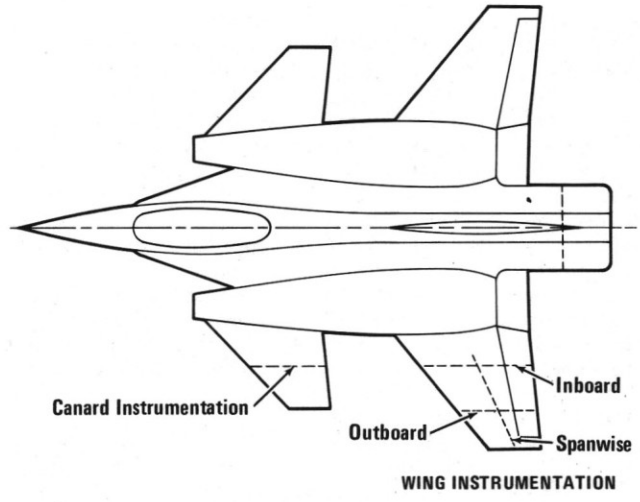

Figure 2 Pressure Instrumentation on the Large-Scale Model

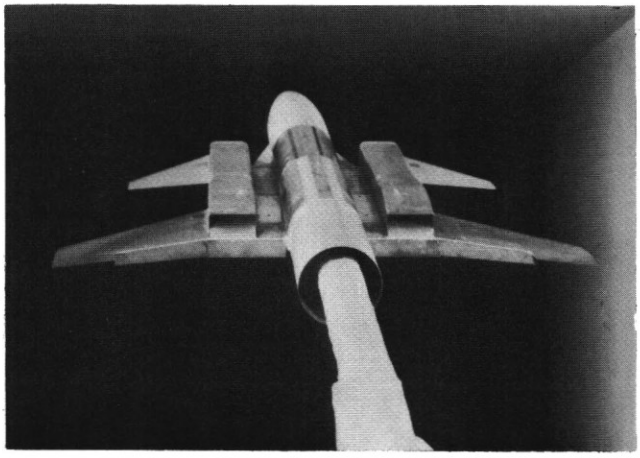

Figure 3 General Dynamics' Small-Scale VEO-Wing Research Model

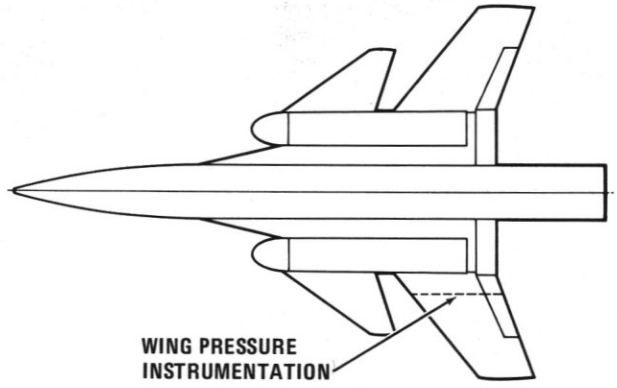

Figure 4 Pressure Instrumentation on the Small-Scale Model

TABLE 2

GEOMETRIC CHARACTERISTICS OF THE SMALL-SCALE MODEL

FUSELAGE	
Length	70 in
WING	
Planform Area	3.50 ft^2
Span	43.5 in
Leading-edge Sweep	40 deg
Aspect Ratio	3.75
Taper Ratio	.4
Twist	-4 deg
Airfoil Section (Exposed Root)	NACA 64A205
Airfoil Section (Tip)	NASA 64A204
CANARD	
Planform Area	.70 ft^2
Span	33.3 in
Leading-edge Sweep	55 deg
Aspect Ratio	2.1
Taper Ratio	.3
Airfoil Section	4% BICONVEX

The nozzle exit on the small-scale model was positioned near the hingeline of the wing trailing-edge flap to obtain thrust turning capability. The basic nozzle was a two-dimensional convergent-divergent plug nozzle with a ramp angle of either 20 deg or 25 deg, depending upon the trailing-edge flap setting. The basic spanwise nozzle for the small-scale model was similar to that of the large-scale model; it had an aspect ratio of 4.0, a sweep angle of 40 deg, and was flush mounted on the outer nacelle wall near the wing upper surface.

In a manner similar to that employed on the large-scale model, the exit area of the chordwise nozzles on the small-scale model was reduced to maintain a constant total exit area when the spanwise nozzles were installed. The spanwise nozzles accounted for approximately 28% of the total exit area.

The small-scale model was tested on a six-component balance in the 7- by 10-Meter Low-Speed Wind Tunnel at the NASA Langley Research Center. In addition to the force data, chordwise pressure data were acquired on the wing along the single row shown in Figure 4. The angle of attack was varied from -4 deg to 24 deg, and the freestream dynamic pressure was 40 psf, which corresponds to a Mach number of approximately 0.166.

DATA CHARACTERISTICS

Large-Scale Model

The basic purpose of this paper is to present the effects of power on the aerodynamic flowfield. However, an understanding of the power-off flowfield is needed before discussing the effects of power. The most significant feature of the large-scale model flowfield was a leading-edge vortex that formed on the wing at low angles of attack and progressively grew stronger and moved inboard as the angle of attack was increased. Figure 5 shows the approximate positions of the vortex centerline at several conditions. The vortex divided the wing flowfield into two regions of distinctly different flow: the flow inboard of the vortex was attached and the flow

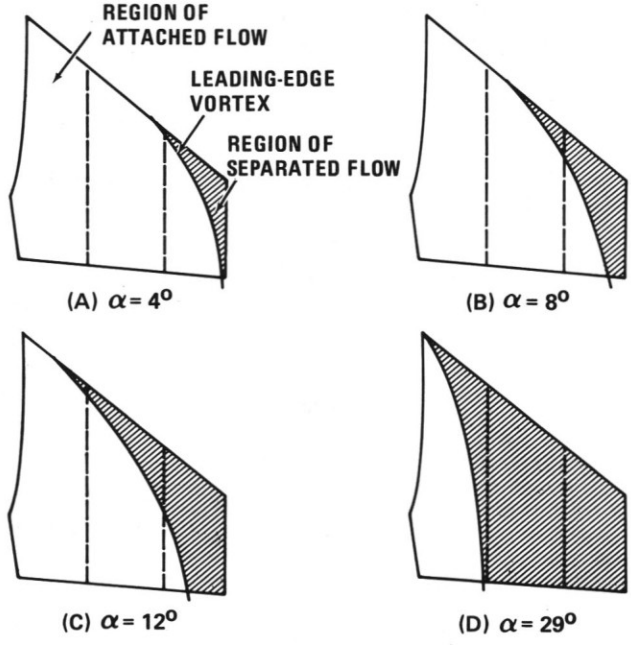

Figure 5 Positions of Wing Leading-Edge Vortex Centerline

outboard of the vortex was separated. Other variables that influenced the wing flowfield (such as the canard setting, the wing trailing-edge-flap setting, and the power setting) also had an effect on the vortex position.

As the vortex passed over the instrumented stations, the pressure distributions exhibited the characteristics shown in Figure 6, which helped identify its position. Figure 6A shows a typical attached-flow pressure distribution of a section inboard of the vortex. Figure 6B shows a pressure distribution which indicates by the high suction peak and the following minor compression that a small but relatively strong portion of the vortex was positioned over the instrumented station. Thus, it follows that the vortex origin was slightly inboard when this shape of the pressure distribution was observed. Figure 6C shows a pressure distribution at a wing station that was beneath a widespread and weak portion of the vortex, as indicated by the bulge between the 30% to 60% chord. At these conditions, the flow was separated near the leading edge and the pressures there were beginning to assume a flat distribution. At some point in this progression, it is certain that the vortex burst, but this action could not be positively identified from the surface pressures. Therefore, this type of pressure distribution is assumed to result from a weak, widespread vortex. Figure 6D shows a flat pressure distribution that was characteristic of the separated flow region outboard of the vortex. The wing vortex was prominent, but not unique; a similar flow pattern also existed on the canard.

Small-Scale Model

The small-scale force model was tested at power settings ranging from $C_T = 0$ to $C_T = 2.0$. Figure 7 shows the thrust-included lift, moment, and drag coefficients for the model to provide a perspective of the magnitudes of the forces involved. At low Mach number, the thrust was a major factor in the forces measured at the balance. For example, when the flaps were deflected, the component of thrust in the lift direction was approximately equal to the aerodynamic lift and the thrust component in the drag direction far exceeded the aerodynamic drag.

The power-induced lift, ΔC_L, was determined by removing, from the power-on lift, the power-off lift and the thrust component in the lift direction. It is computed by the equation

$$\Delta C_L = C_{L_{Power\ On}} - C_{L_{Power\ Off}} - C_T \sin(\alpha + \theta_j) \qquad \text{(Equation 1)}$$

Since lift is a critical aerodynamic parameter for STOL operation, it is used almost exclusively in this paper to illustrate the effects of power on the small-scale force model.

CHORDWISE BLOWING

Large-Scale Model

The chordwise blowing effects on the wing pressures at the inboard station are shown in Figure 8 for an angle of attack (alpha) of 17 deg. This figure shows the data points in order to indicate the chordwise positions of the orifices from which the pressure distributions were established since the remainder of the pressure plots for this model are presented without the data points. Figure 8 also shows the effects on both the upper and lower wing surfaces of chordwise power (blowing); the effect shown for the lower surface is one of the largest that was observed on this model. Typical lower-surface pressure changes due to power were only a fraction of the amount shown and diminished to an insignificant amount at both the lower and higher alphas. Hence, the following discussion is limited to the predominant upper-surface pressures. Both upper-surface and lower-surface pressure changes due to power were decreases (almost without exception), which indicates that exhaust jet entrainment created an acceleration of the flow over both surfaces.

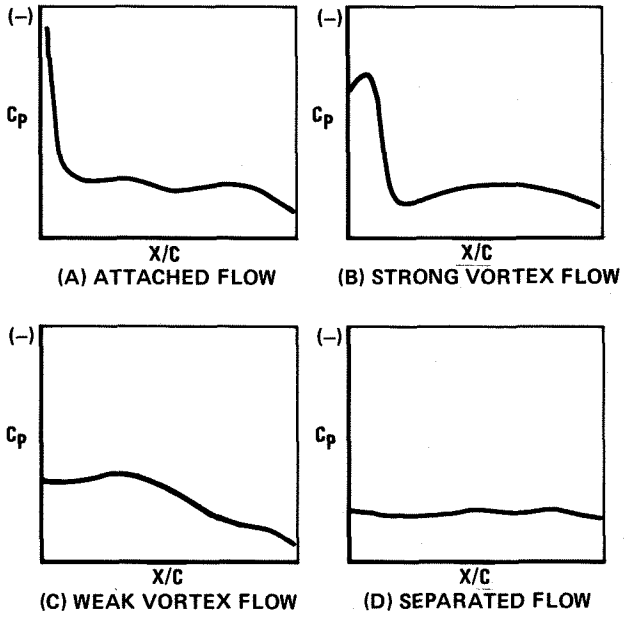

Figure 6 Characteristics of the Pressure Distributions Beneath the Wing Leading-Edge Vortex

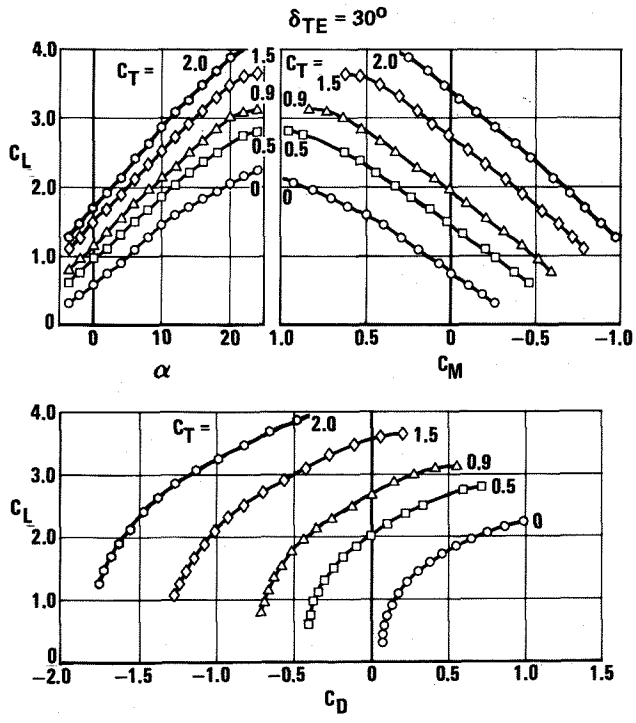

Figure 7 Thrust-Included Forces on the Small-Scale Model

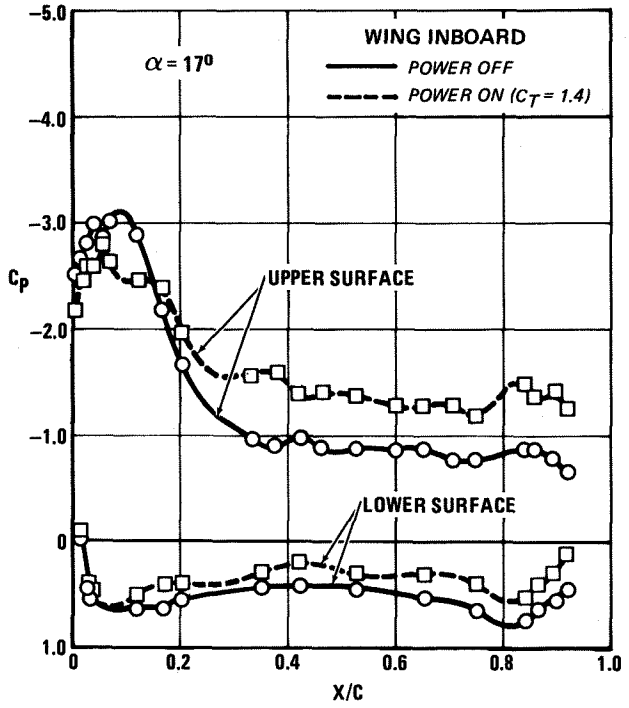

Figure 8 Effects of Chordwise Blowing on the Wing Upper-and Lower-Surface Pressures

Figure 9 shows chordwise blowing effects on the canard and wing upper-surface pressures at four angles of attack and a deflected trailing-edge flap. The attached and separated flow regions and the movement of the vortices are discussed below. The following comments on the power-off case may be related to the wing vortex centerline paths shown in Figure 5.

Alpha = 4 deg. The low pressures on the forward 20% of the canard (Figure 9A) were caused by a weak canard leading-edge vortex that originated on the surface just inboard of the instrumented station. The influence of power on the canard vortex position and canard pressures was small at this alpha. Flow at the inboard wing station was attached for both power-on and power-off conditions, but the pressures were substantially more negative for the power-on case. The wing leading-edge vortex was positioned near the mid-span, and although it was very weak at this alpha, it caused a small region of low pressure near the leading-edge of the outboard wing station. When power was applied, the vortex moved inboard slightly, but became stronger and developed a higher, better defined suction peak at the leading edge of the outboard station. The flow over the spanwise station was attached, except very near the wing tip, where the action of the vortex decreased the pressure slightly when the power was off and to a greater degree when the power was on. At this alpha, the power decreased the wing pressures almost uniformly and caused the weak leading-edge vortex to move slightly inboard.

Alpha = 8 deg. The canard leading-edge vortex at this alpha (Figure 9B) was more widespread over the instrumented station than at the alpha of 4 deg, and the chordwise power caused a small decrease in the upper-surface pressures. The flow at the wing inboard station was attached over the entire chord and indicated approximately the same lift increase due to power as at the lower alpha. The shape of the pressure distribution at the outboard station changed substantially when power was applied. With power off, the small, intense portion of the vortex near its origin was positioned over the outboard station. Adding power caused an inboard movement of the vortex and resulted in a more widespread and weaker portion of the vortex being positioned over that station. This does not imply that the vortex was weaker with power on, but only that a different segment of the vortex affected the pressures at the outboard station. The enlargement of the low-pressure region near the tip of the spanwise distributions also supports the concept that the vortex moved inboard when power was applied.

Alpha = 12 deg. The canard vortex was barely discernible at this alpha, but the slope of the canard pressure distribution in Figure 9C indicates that it was substantially inboard of the instrumented station and that it was weak as it swept over that station in an outboard and downstream direction. When the power was applied, there was a uniform reduction in the canard upper-surface pressures but no apparent movement of the vortex. Chordwise power did not appear to move the wing vortex, but it increased its strength and decreased the pressures in the attached-flow region of the inboard station between the vortex and the wing trailing edge. The outboard pressures indicate a widespread and weak vortex with possibly some reattachment of the flow near the trailing edge. The spanwise data show that the vortex was positioned near the 80% span station. Comparison with the spanwise data at lower alphas clearly shows the inboard progression of the vortex as alpha increased.

Alpha = 29 deg. Figure 9D shows that both the canard and wing flowfields were separated at this alpha and that there was no evidence of a vortex on either the canard or the wing. The chordwise power, however, caused a very large decrease in the upper-surface pressures.

Section Lift. Section lift coefficients obtained from integrations of the upper- and lower-surface chordwise pressure distributions of the canard and wing are shown for two flap settings in Figure 10. The section lift coefficients for the wing flaps deflected (Figure 10B) correspond with the pressure data presented in Figure 9. With the wing flaps neutral and alphas below the stall angle (Figure 10A), the canard and wing lift increased moderately when power was applied. Above the stall angle, there was a very large increase in the lift on both the canard and the wing. With flaps deflected (Figure 10B), power effects on the canard lift were about the same as with flaps neutral, but the effects on the wing lift were significantly larger. At the high alphas, the influence of power on both the canard and wing was quite large, suggesting that power effects in this range were not strongly dependent upon the flap setting. Supporting evidence that the power effects were widespread and almost uniform over both surfaces was that neither the wing or canard section center of pressure changed significantly when power was applied.[7]

Small-Scale Model

The wing pressure data from the small-scale model support the conclusions about power effects that were drawn from the large-scale model pressure data, i.e., that power effects on the lower surface were minimal, while on the upper surface a significant and widespread reduction in pressure occurred. Pressure data on the upper surface of the small-scale model wing (Figure 11) show typical power effects that extend from leading edge to trailing edge.

The pressure data suggest that a wing leading-edge vortex was also present on the small-scale model. The wing pressure instrumentation, however, was closer to the

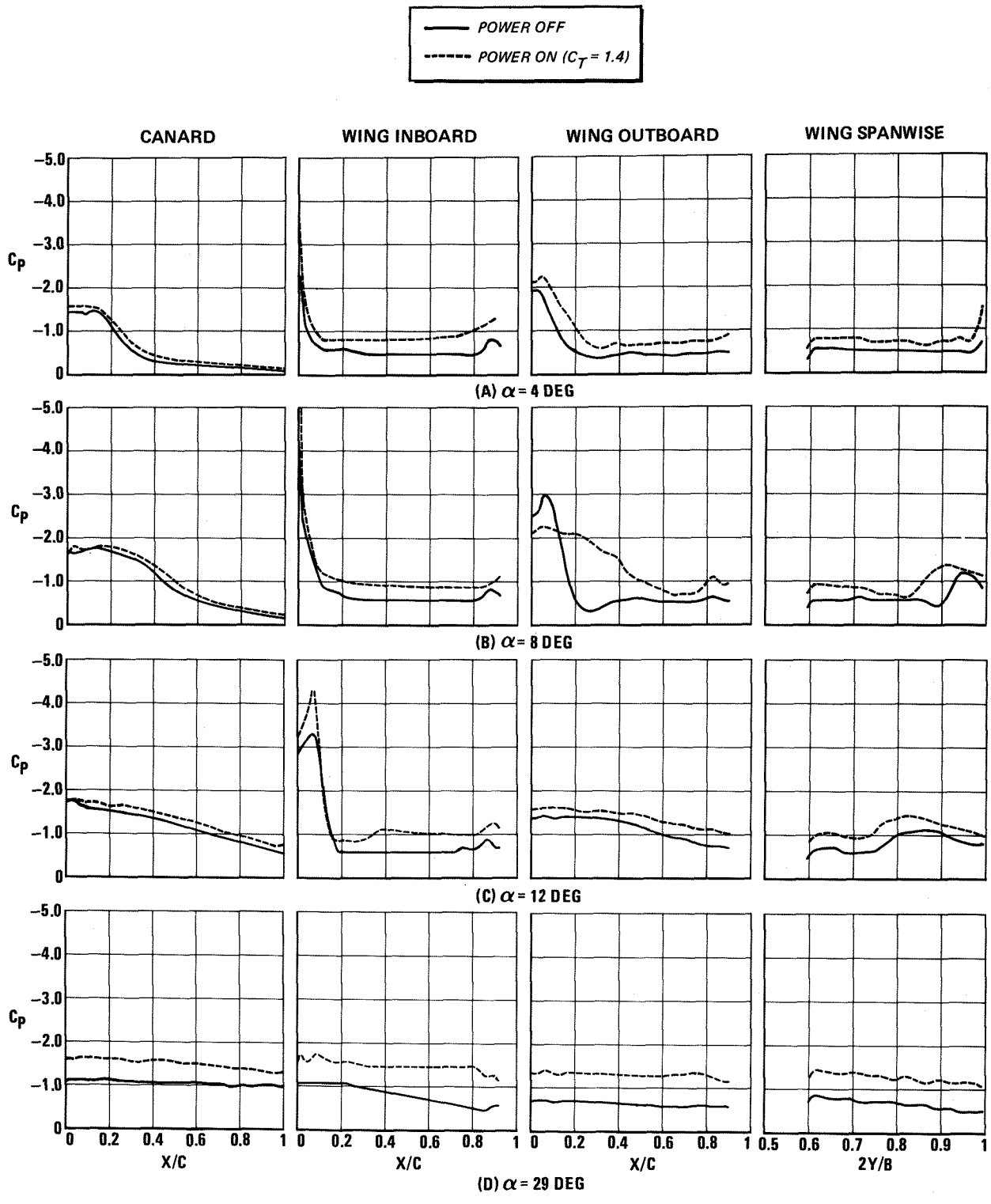

Figure 9 Chordwise Blowing Effects on the Wing and Canard Upper-Surface Pressures, δ_{TE} = 30°

side of the nacelle and there were fewer orifices near the leading edge than on the large-scale model. Therefore, it could not be concluded whether the vortex was less significant on the small model or if its influence was simply not as apparent because of the location of the instrumentation.

Power-induced lift increments measured by the force balance are shown in Figure 12 for a C_T of 2.0. These lift increments basically reflect an increase in the lift-curve slope for flaps neutral and an incremental shift in the lift curve for flaps deflected. In either case, the total aerodynamic lift at high alphas was increased sub-

stantially by chordwise blowing. Figure 13 shows a typical variation of the power-induced lift as the thrust level was increased. Most of the aerodynamic benefits were obtained with a value of C_T as low as 1.0.

SPANWISE BLOWING

Large-Scale Model

Spanwise blowing (SWB) on the upper surface of the wing caused very large changes in the pressure distributions, as shown in Figure 14. Direct effects of the SWB jet were low-pressure regions beneath its path; indirect effects were primarily its influence on the strength and position of the wing leading-edge vortex. Each of these effects is indicated by the data in Figure 14. The SWB-off data in this figure are for power on, but with all the engine flow directed through the chordwise nozzles. The

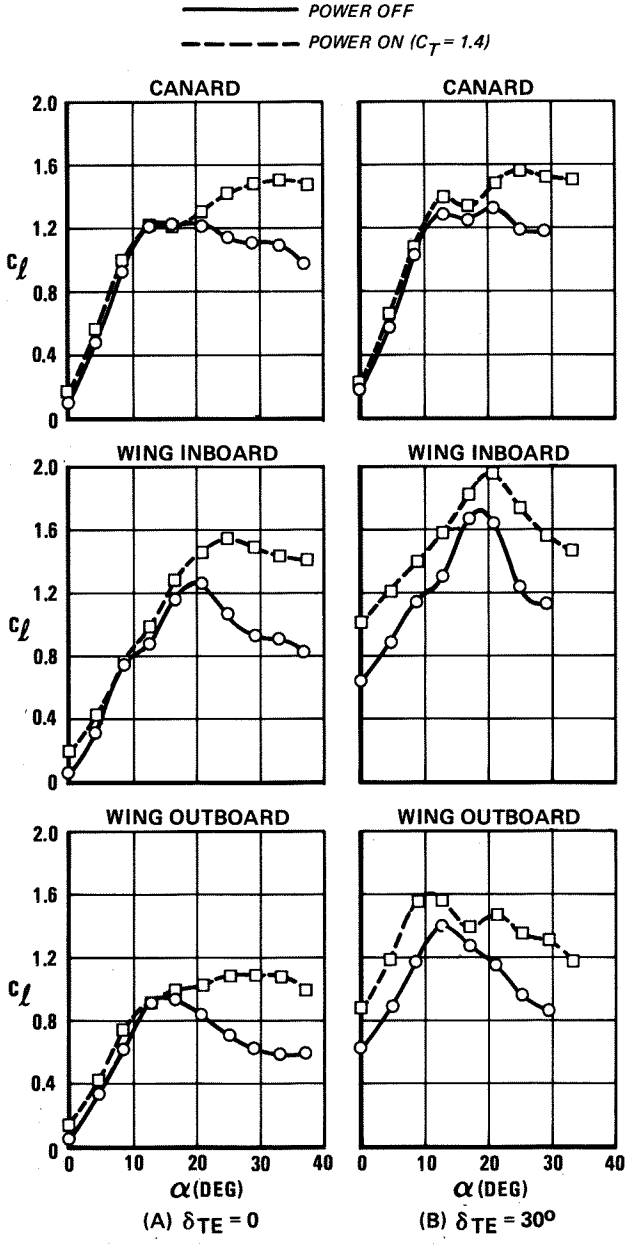

Figure 10 Chordwise Blowing Effects on the Wing and Canard Section Lift Coefficients

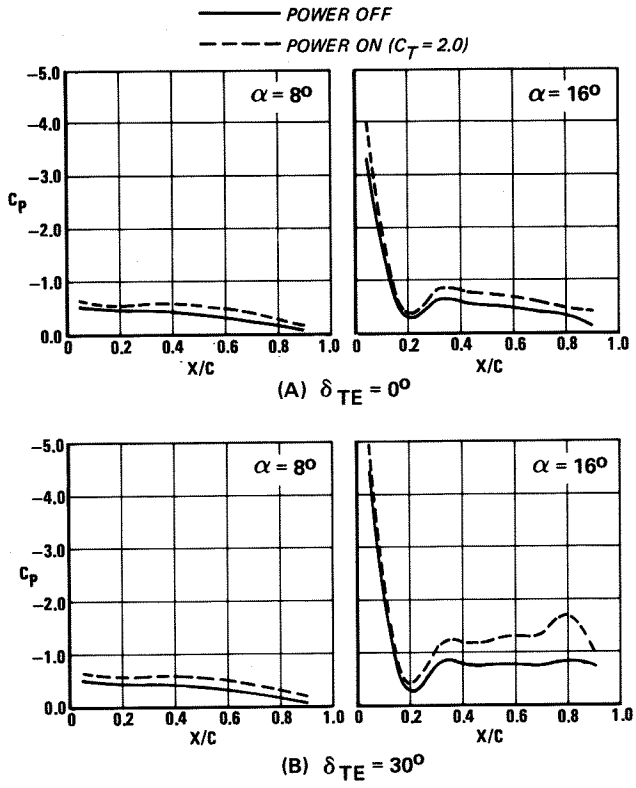

Figure 11 Effects of Chordwise Blowing on the Wing Pressures of the Small-Scale Model

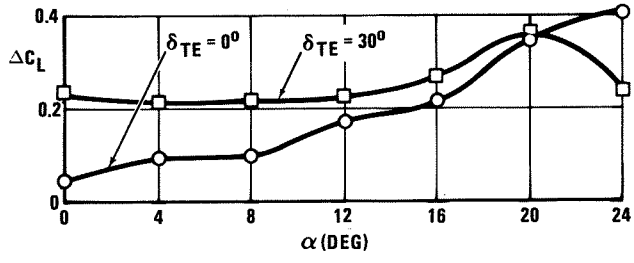

Figure 12 Power-Induced Lift Increments on the Small-Scale Model, C_T = 2.0

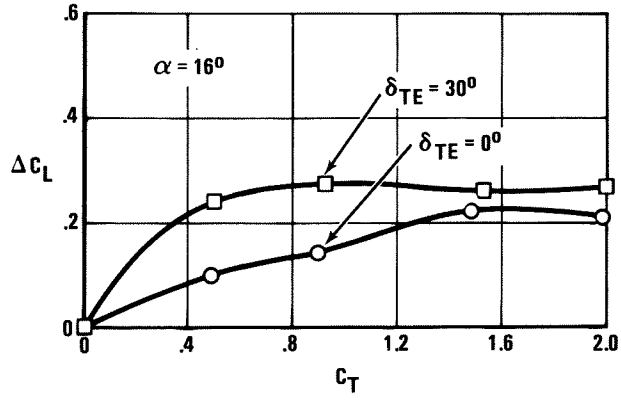

Figure 13 Power-Induced Lift Increments on the Small-Scale Model, Alpha = 16 Degrees

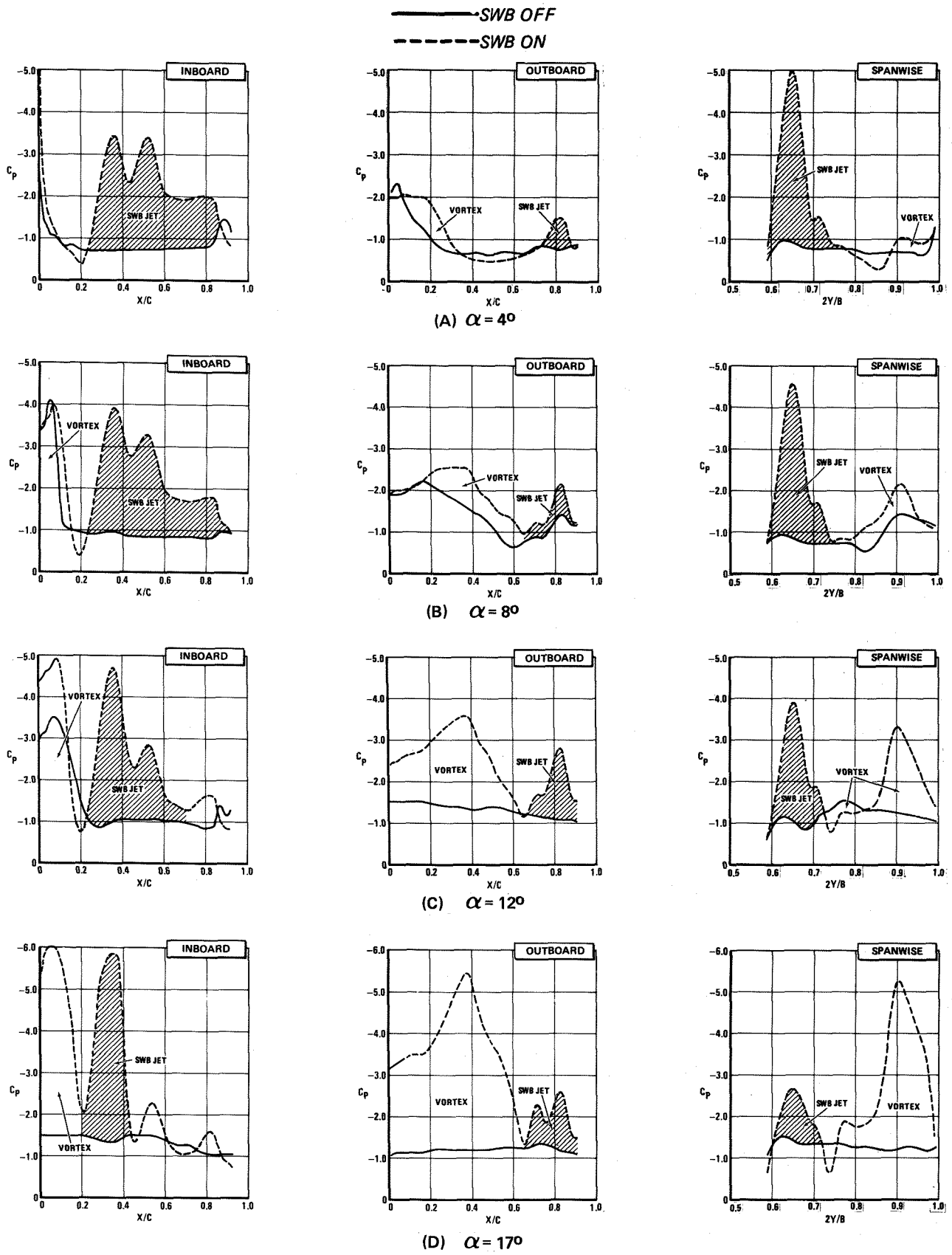

Figure 14 Spanwise Blowing Effects on the Wing Upper-Surface Pressures

SWB-on data are for the same total engine flow but with approximately 17% of the flow diverted through the SWB nozzles.

Alpha = 4 deg. Low-pressure regions in Figure 14A show that the SWB jet was positioned between the 25% and 85% chord of the inboard station, near the trailing edge of the outboard station, and between the 60% and 75% spanwise stations. The wing leading-edge vortex was positioned near the tip with SWB off and was further inboard with SWB on.

Alpha = 8 deg. At this alpha (Figure 14B), the SWB jet was in approximately the same position as it was at a 4-deg alpha. The wing vortex was further inboard and produced a strong suction on the leading edge of the inboard station for SWB either on or off. The outboard and spanwise stations both show that the wing vortex was stronger with SWB on.

Alpha = 12 deg. The suction effects of the SWB jet at this alpha were smaller near the trailing edge of the inboard station but larger near the trailing edge of the outboard station (Figure 14C). This indicates that the jet was deflected less by the freestream flow and penetrated further in the spanwise direction. The SWB jet increased the strength of the vortex and caused it to move in an outboard direction. At the inboard station, the increased vortex strength is quite evident. Pressure data at the outboard station show the significance of the SWB enhancement of the vortex as it moved from a position inboard of that station (SWB off) to a position above that station (SWB on). The spanwise data also show that the vortex was further outboard and stronger with SWB on.

Alpha = 17 deg. The flat pressure distributions of Figure 14D indicate that the flow was separated without spanwise blowing. With SWB on, the jet traversed the inboard station between the 20% and 45% chord, indicating that it was deflected less than at any lower alpha. The SWB jet provided strong enhancement of the leading-edge vortex, creating large areas of low pressure at all three instrumented wing stations.

Section Lift. Figure 15 shows the effects of SWB on the section lift coefficients obtained from integrations of the wing pressure data. At low alphas, most of the lift increase resulted from the direct suction effects of the SWB jet, which was strong at the inboard station but weak at the outboard station since it barely penetrated that far. At the high alphas, the enhanced vortex was primarily responsible for the lift increases. At the best alpha for spanwise blowing (21 deg), the section lift was increased by 110% at the inboard station and by 170% at the outboard station. The section center of pressure moved forward at the high angles of attack when SWB was applied. This correlates well with the flowfield depiction of spanwise blowing enhancing the leading-edge vortex.

Thermal Effects of SWB. Isotherm patterns in the flowfield of the SWB jet and the upper surface of the large-scale model wing are shown in Figure 16. Isotherm, in this context, is defined to be the incremental temperature increase of the flow above the freestream temperature. With an engine operating temperature of approximately 1100°F, the maximum temperature increase measured on the wing was about 200°F at the low alphas and about 300°F at the high alphas. Instrumentation closer to the SWB nozzle would have obviously measured higher temperatures. The vortex centerline paths, as determined from the pressure data, are also shown in Figure 16.

Figure 16A characterizes the positions of the vortex and the SWB jet at low alphas. They were roughly parallel but widely separated. At an 8-deg alpha (Figure 16B) the SWB was less swept and the vortex was positioned farther inboard, placing the two flows much closer together. The

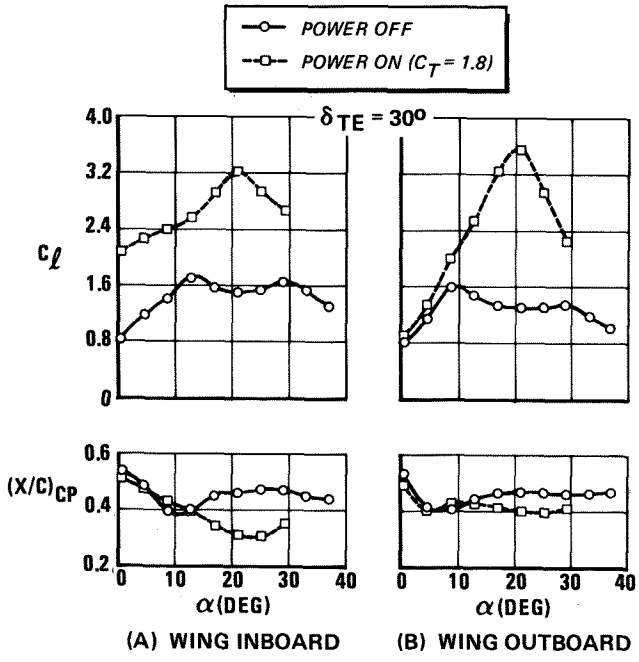

Figure 15 Spanwise Blowing Effects on the Wing Section Lift Coefficients and Center of Pressure

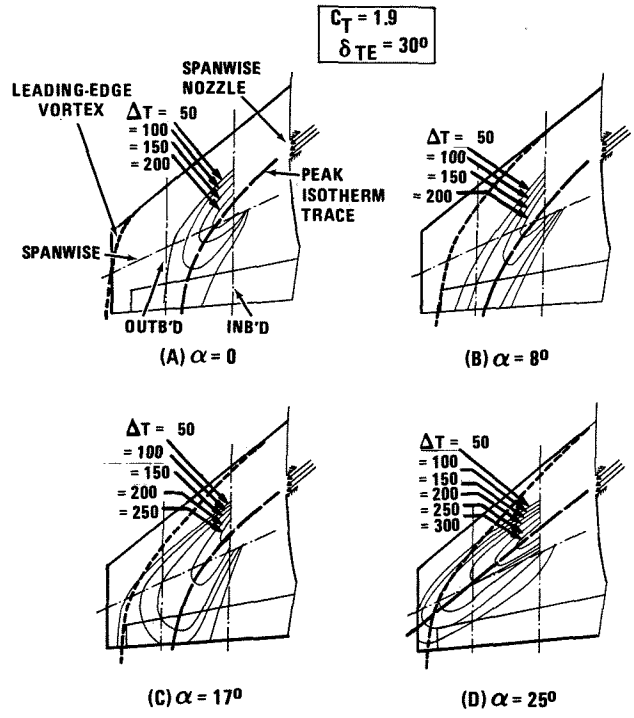

Figure 16 Isotherm Patterns Due to Spanwise Blowing with Hot Gases

flow patterns maintained these general characteristics through an alpha of 17 deg (Figure 16C), except that the SWB jet was spread over a larger area at the higher alpha. Between 21 deg and 29 deg the isotherms are characterized by the 25-deg data in Figure 16D. The suction of the wing leading-edge vortex acting in a basically separated wing flowfield pulled the SWB jet forward. The SWB jet and the vortex centerline paths appear to intersect in the planform view, but the jet was near the surface of the wing and the vortex was positioned above it. Thus, the SWB jet and the wing leading-edge vortex acted peripherally throughout the alpha range, but the two flows never became confluent.

Small-Scale Model

Spanwise blowing proved to be an effective means for increasing the lift of the small-scale model. The power-induced lift increment with SWB on is compared in Figure 17 with the lift increment for chordwise blowing only. The lift increment with chordwise blowing only was almost constant across the alpha range, but the SWB-on lift increment increased significantly with alpha (Figure 17a). Both cases reached a thrust level at which additional power did not increase the lift (Figure 17b). This occurred at a higher thrust when the SWB was employed.

Strong synergistic interactions occurred between the chordwise and spanwise jets at some conditions. With the wing flaps neutral (Figure 18A), the favorable effects were limited to thrust levels above a C_T of 3.0. With the wing flaps deflected (Figure 18B) the interactions between the two flows increased the lift by about 40% over the thrust range.

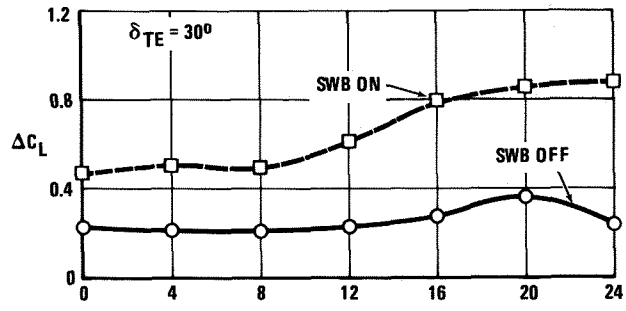

(A) $C_T = 2.0$

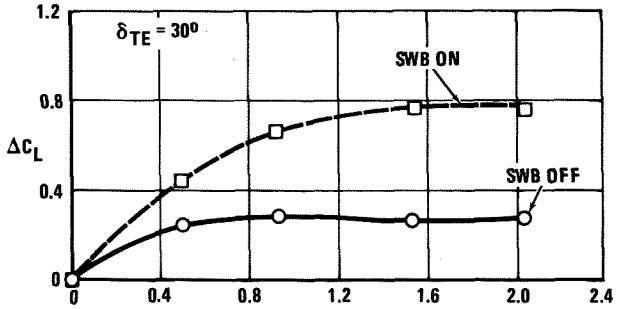

(B) $\alpha = 16°$

Figure 17 Power-Induced Lift Due to Chordwise and Spanwise Blowing

NOZZLE CONFIGURATION EFFECTS

Chordwise Nozzles

Six sets of 2-D chordwise nozzles were tested on the small-scale model to determine nozzle configuration effects on the power-induced aerodynamics. Figure 19 illustrates the nozzle configurations and specifies the expansion area ratios and the exit plane longitudinal positions relative to the wing root chord. (Results shown earlier were with the A nozzle.) Test results of NPR variations at static freestream conditions (Figure 20) show that all the nozzles produced approximately the same thrust levels and turning angles. The ramp angle and the flap upper-surface angle were both set at 20 deg, and the measured thrust deflection angle ranged from 18 deg to 23 deg at an NPR of 3.0. At this NPR ($C_T \cong 2$), the thrust variation was between ± 3% of the average value. Thrust calibrations based on these data were used in the computation of the power-induced lift coefficients (Equation 1).

The power-induced aerodynamic lift coefficient developed at a 16-deg alpha with each of the nozzle configurations is shown in Figure 21. At the higher thrust levels, the convergent nozzle (D) provides the most induced lift. All of the jet expansion occurs outside this nozzle, and it was probably large values of freestream entrainment into the jet that accelerated the flow and caused the convergent nozzle to be the most effective in inducing lift. The nozzles with the exit planes near the

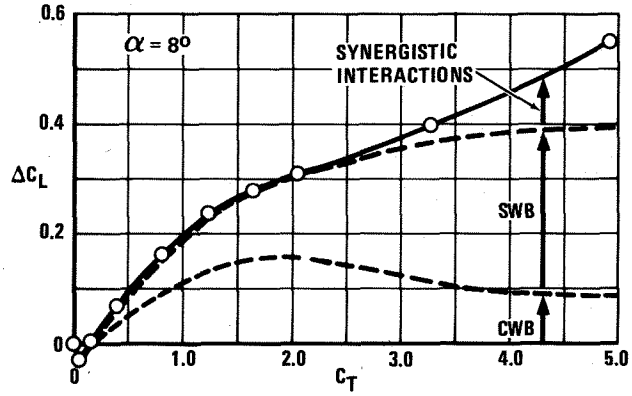

(A) $\delta_{TE} = 0°$

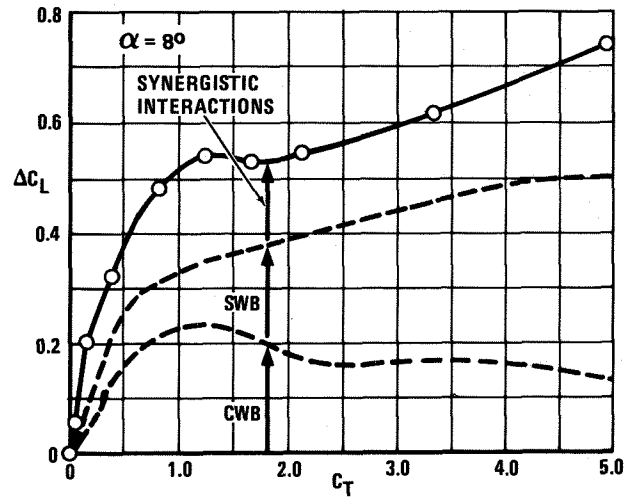

(B) $\delta_{TE} = 30°$

Figure 18 Synergistic Interactions of Chordwise and Spanwise Blowing

wing trailing edge (E and F) place the exhaust jet farther from the wing flowfield and, hence, produce less induced lift than the other nozzles. Nozzles A, B, and C produced results that were near the mid-point of the high and low values produced by the other nozzles.

Figure 22 shows the relative magnitudes of the thrust component in the lift direction and the power-induced aerodynamic lift at a 16-deg alpha and a 15-deg trailing-edge flap. The thrust lift was significantly larger than the induced lift. However, the point of application of the thrust lift was near the nozzle exit, resulting in a large nose-down moment. On the other hand, the induced lift was distributed over the model and perhaps could be more easily trimmed. A similar comparison at trimmed conditions would probably be more favorable for the power-induced lift. The convergent nozzle (D) displayed the most total lift as well as the most induced lift. The thrust-included lift coefficients of all the nozzles ranged from 98% to 110% of the lift coefficient of the basic nozzle (A).

Spanwise Nozzles

The small-scale model was tested with four sets of spanwise nozzles to determine the effects of the nozzle shape, size, and sweep angle on the power-induced aerodynamics. Table 3 lists the basic geometric parameters for each of the spanwise nozzles. The aspect ratio of the rectangular nozzles, which were flush with the external contour of the nacelle, was 4.0. The round nozzles were mounted on the nacelles at the same location but extended approximately 1.4 inches into the freestream flow.

The lift induced with each of the spanwise nozzles in combination with the basic chordwise nozzle (Config. A) is shown in Figure 23 for an alpha of 16 deg. All of the spanwise nozzles with a 1.0-in^2 exit area induced almost equal values of lift at the low alphas. But at alphas of 16 deg and above, the rectangular nozzle with the 40-deg sweep angle (Config. 1) was somewhat more effective than the others. The round nozzle with the 0.5-in^2 exit

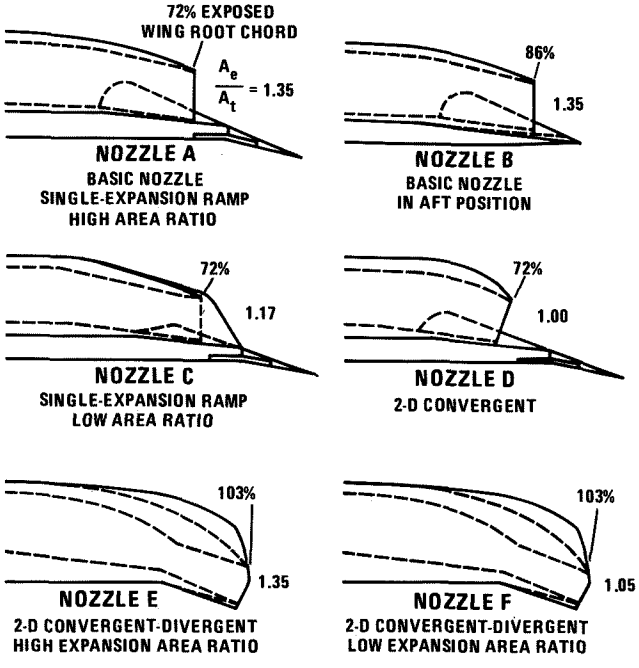

Figure 19 Chordwise Nozzle Configurations

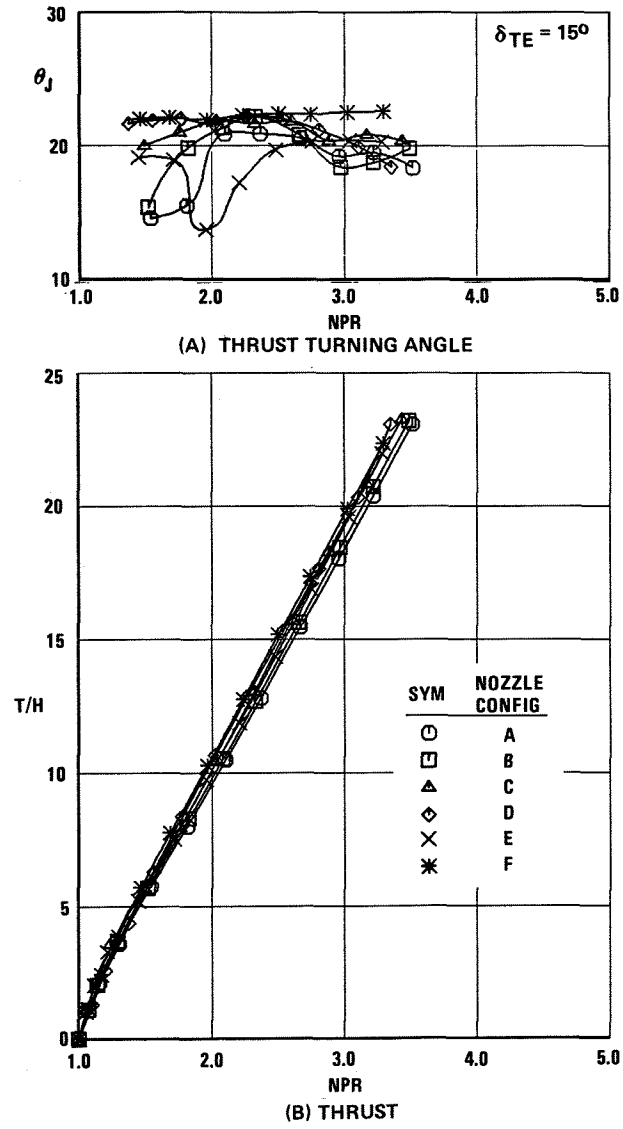

Figure 20 Performance of Chordwise Nozzles at Static Freestream Conditions

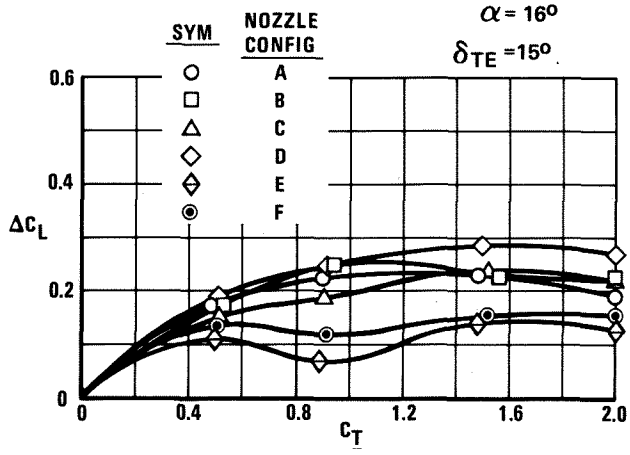

Figure 21 Chordwise Nozzle Configuration Effects on Power-Induced Lift

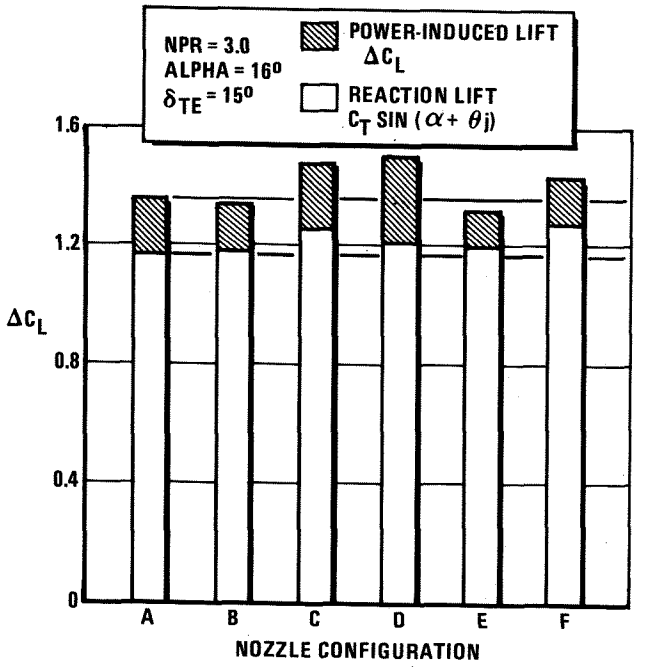

Figure 22 Comparison of the Thrust-Included Lift Coefficients for the Chordwise Nozzles

TABLE 3

GEOMETRIC CHARACTERISTICS OF SPANWISE NOZZLES

CONFIG. NO.	GEOMETRIC SHAPE	SWEEP (deg)	EXIT AREA (in^2/side)
1	Rectangular	40	1.0
2	Rectangular	60	1.0
3	Round	40	1.0
4	Round	40	0.5

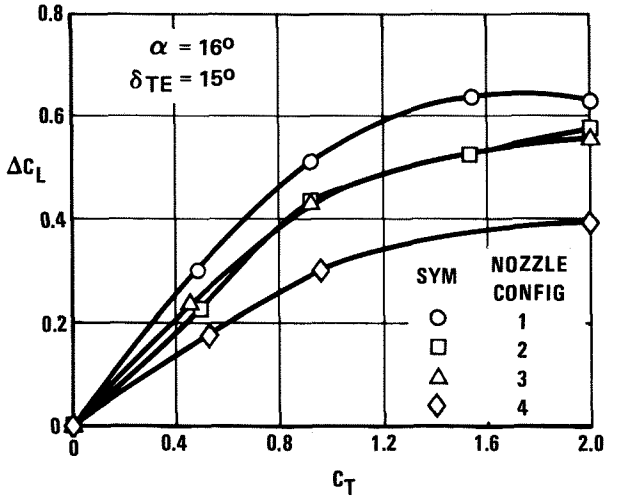

Figure 23 Spanwise Nozzle Configuration Effects on the Power-Induced Lift

area was the least effective at all alphas. Its relationship to the other nozzles, shown in Figure 23, is typical of all alphas. The lift induced by the aft-swept rectangular nozzle (Config. 2) and the round nozzle (Config. 3) was between that of the other two nozzles. The effects of the Config. 2 and 3 spanwise nozzles were remarkably similar across the alpha and C_T ranges that were tested.

CONCLUSIONS

Several general conclusions may be derived from the collective data of the large-scale and small-scale models. Configuration differencies are not felt to be of major impact on the characteristics of the force data or the behavior of the flowfield because of the similarity of the wing/canard/nacelle arrangements. And even though the instrumentation differencies preclude a direct data comparison for scale effects, it is felt that the conclusions apply to both models, with one possible exception - the wing leading-edge vortex, which may have a larger influence on the flowfield of the large-scale model.

The pressure data show the effects of a leading-edge vortex on the wing that begins near the tip and moves inboard as alpha is increased, dividing regions of attached flow inboard of the vortex and separated flow outboard of the vortex. Thus, the areas of the wing exposed to attached and separated flows can be determined from the vortex position. The position of the vortex is also affected by both chordwise and spanwise blowing. Since the vortex causes localized disturbances in the flowfield, its movements and influence on the pressure patterns must be considered when evaluating power effects.

Chordwise blowing effects on the wing pressures are small on the lower surface but significant, widespread, and favorable on the upper surface. Wing chordwise blowing also reduces the canard upper-surface pressures — slightly at low alphas but by a large amount at alphas above the stall angle.

Spanwise blowing clearly enhances the strength of the leading-edge vortex, which results in very large pressure decreases beneath its path. The path of the spanwise jet, as determined from the thermal data, show that it is basically parallel to the vortex at low alphas and passes beneath the vortex at high alphas. Thus, the vortex flow and the spanwise jet are never confluent. A more efficient arrangement could possible be achieved by repositioning the spanwise nozzle to allow the jet and vortex flows to merge.

The lift induced by chordwise blowing depends on the angle of attack and the flap setting. At typical STOL conditions, the lift coefficient is increased by 0.2 to 0.3, most of which could be obtained with C_T values below 1.0. With simultaneous chordwise and spanwise blowing, the lift coefficient is increased by about 0.8 at STOL conditions. This high value results in part from strong synergistic interactions between the two flows.

The shape of the nozzles had a moderate influence on the power-induced lift. The convergent nozzle provided the most induced lift from chordwise blowing, which may have been caused by the jet expansion occurring outside this nozzle, thereby developing a higher entrainment of the freestream flow. The 40-deg-sweep, rectangular nozzle was the best spanwise nozzle.

Chordwise and spanwise blowing for low-speed lift augmentation appears encouraging from an aerodynamic

standpoint. Although large values of lift forces can be obtained through thrust deflection, the power-induced forces may be more usable because of trim requirements. The true potential of chordwise and spanwise blowing for increasing STOL performance can only be determined through evaluation of the concepts when integrated into an aircraft design.

ACKNOWLEDGEMENTS

The model tests and the data analyses reported in this paper are the products of coordinated efforts of a large number of persons in several organizations. The author wishes to acknowledge the major contributors: Mr. Michael D. Falarski of the NASA Ames Research Center for his efforts in the design and testing of the large-scale STOL fighter model; Mr. John W. Paulson, Jr. of the NASA Langley Research Center for his efforts in the testing of the General Dynamics small-scale research model; and Mr. Stephen C. Stumpfl of the Air Force Flight Dynamics Laboratory for coordinating the activities of the organizations involved in the testing and evaluation of the small-scale model and for developing some of the data reduction techniques that were unique to this model.

REFERENCES

1. Woodrey, R. W., Whitten, P. D., Smith, C. W., and Bradley, R. G., "An Experimental Investigation of a Vectored-Engine-Over-Wing Powered-Lift Concept, Volume I — Low Speed and Transonic Test," AFFDL-TR-76-92, September 1976.

2. Whitten, P. D., "An Experimental Investigation of a Vectored-Engine-Over-Wing Powered-Lift Concept, Volume II —High Angle of Attack and STOL Tests," AFFDL-TR-76-92, March 1978.

3. Leavitt, L. D., "Longitudinal Aerodynamic Characteristics of a Vectored-Engine-Over-Wing Configuration at Subsonic Speeds," NASA Technical Paper 1533, October 1979.

4. Stumpfl, S. C., "Longitudinal Aerodynamic Data for an Unpowered 1/15-Scale Vectored Engine-Over-Wing Configuration Model," AFWAL-TM-80-80-FIMM, August 1980.

5. Whitten, P. D. and Howell, G. A., "Investigations of the VEO-Wing Concept in an Air-to-Ground Role," AFFDL-TR-79-3031, March 1979.

6. Howell, G. A., "Low-Speed Wind Tunnel Investigations of the Vectored-Engine-Over-Wing Concept with Podded Nacelles," AFWAL-TR-82-3009, March 1982.

7. Howell, G. A., Crosthwait, E. L., and Witte, M. C., "Evaluation of Pressure and Thermal Data From a Wind Tunnel Test of a Large-Scale, Powered, STOL Fighter Model," NASA CR-166170, June 1981.

8. Falarski, M., Dudley, M., and Howell, G., "Analysis of Data From a Wind Tunnel Investigation of a Highly Maneuverable Supersonic V/STOL Fighter: STOL Configuration," AIAA Paper No. 81-2620, December 1981.

9. Harris, M. J. and Falarski, M. D., "Static Calibration of a Two-Dimensional Wedge Nozzle With Thrust Vectoring and Spanwise Blowing," NASA Technical Memorandum 81161, April 1980.

10. Falarski, M. D., Whitten, P. D., and Harris, M. J., "Aerodynamic Characteristics of a Large-Scale Model of a Highly Maneuverable Supersonic V/STOL Fighter: STOL Configuration," AIAA Paper No. 80-0234, January 1980.

11. Wray, W. O., Jr., "Model and Test Information Report, 0.108-Scale Powered Lift Research Model for NASA Langley Research Center," General Dynamics Report FZT-259, Addendum III, December 1, 1978.